

# The state space and physical interpretation of self-similar spherically symmetric perfect-fluid models

B. J. Carr<sup>‡</sup>, A. A. Coley<sup>§</sup>, M. Goliath<sup>||</sup>, U. S. Nilsson<sup>¶</sup> and C. Uggl<sup>+</sup>

**Abstract.** The purpose of this paper is to further investigate the solution space of self-similar spherically symmetric perfect-fluid models and gain deeper understanding of the physical aspects of these solutions. We achieve this by combining the state space description of the homothetic approach with the use of the physically interesting quantities arising in the comoving approach. We focus on three types of models. First, we consider models that are natural inhomogeneous generalizations of the Friedmann Universe; such models are asymptotically Friedmann in their past and evolve fluctuations in the energy density at later times. Second, we consider so-called quasi-static models. This class includes models that undergo self-similar gravitational collapse and is important for studying the formation of naked singularities. If naked singularities do form, they have profound implications for the predictability of general relativity as a theory. Third, we consider a new class of asymptotically Minkowski self-similar spacetimes, emphasizing that some of them are associated with the self-similar solutions associated with the critical behaviour observed in recent gravitational collapse calculations.

PACS numbers: 0420, 0420J, 0440N, 9530S, 9880H

## 1. Introduction

Spherically symmetric self-similar (SSS) perfect-fluid solutions to Einstein's equations have attracted considerable attention over the last two decades. Although a nearly complete classification of such solutions has now been achieved, many of their features remain obscure. The aim of this paper is to provide a better understanding of the solution space and to unravel some of the physical properties of the solutions.

There are a number of preferred geometric structures exhibited by the models, and these have led to several different approaches. Two of the most commonly used are the 'comoving' approach and the 'homothetic' approach. In the comoving

<sup>‡</sup> Astronomy Unit, Queen Mary and Westfield College, University of London, Mile End Road, London E1 4NS, England. E-mail: B.J.Carr@qmw.ac.uk

<sup>§</sup> Department of Mathematics and Statistics, Dalhousie University, Halifax, Nova Scotia, B3H 3J5, Canada. E-mail: aac@mscs.dal.ca

<sup>||</sup> Department of Physics, Stockholm University, Box 6730, S-113 85 Stockholm, Sweden. E-mail: goliath@physto.se

<sup>¶</sup> Department of Applied Mathematics, University of Waterloo, Waterloo, Ontario N2L 3G1, Canada. E-mail: unilsson@mercator.math.uwaterloo.ca

<sup>+</sup> Department of Physics, University of Karlstad, S-651 88 Karlstad, Sweden. E-mail: uggl@physto.se

approach, pioneered by Cahill & Taub [1], the coordinates are adapted to the fluid 4-velocity vector, whereas in the homothetic approach, introduced by Bogoyavlensky and coworkers [2, 3], they are adapted to the homothetic vector. The main advantage of the homothetic approach as presented by Goliath et al. ([4, 5]; GNU1, GNU2) is that the state space is compact and regular. However, physically interesting quantities are more straightforward to obtain in the comoving approach, as shown by Carr & Coley ([6, 7, 8]; CC). It is therefore clear that the two approaches are complementary, and consequently both will be used in this paper.

The outline of the paper is as follows. In section 2 we briefly summarize and compare the approaches of CC and GNU; the discussion here is primarily qualitative, with most of the mathematics being relegated to Appendix A. One new result presented in this section is the complete state space for the SSS models (see figure 6). In section 3 we focus on solutions of particular physical interest: the asymptotically Friedmann models; the so-called asymptotically quasi-static models, of which the naked-singularity solutions studied by Ori & Piran ([9]; OP) are examples; and a class of ‘asymptotically Minkowski’ solutions. We also mention the ‘critical’ solution which has been discovered in gravitational collapse calculations, although we discuss this in more detail elsewhere [10]. A particularly interesting feature of SSS solutions is the way in which their characteristics change at certain critical equations of state and we list these equation-of-state dependent features in section 4. Section 5 contains some concluding remarks and indicates possible future research directions. The governing equations of both approaches are given in Appendix A, together with expressions for some physically interesting quantities.

## 2. Geometric structures

In this section, we summarize the approaches of CC and GNU and discuss their relationship. We will consider an energy-momentum tensor of perfect-fluid form

$$T^{\mu\nu} = \mu u^\mu u^\nu + p(g^{\mu\nu} - u^\mu u^\nu), \quad (1)$$

where  $\mu$  is the energy density,  $p$  is the pressure,  $u^\mu$  is the 4-velocity of the fluid and we choose units for which  $c = 1$ . The only barotropic equation of state compatible with the similarity ansatz is one of the form  $p = \alpha\mu$ , where  $\alpha$  is a constant [1]. Causality requires  $-1 \leq \alpha \leq 1$ . We will confine ourselves to positive pressure and the parameter interval  $0 < \alpha < 1$ .

### 2.1. The comoving approach

In the spherically symmetric situation one can introduce a time coordinate  $t$  such that surfaces of constant  $t$  are orthogonal to fluid flow lines and comoving coordinates  $(r, \theta, \phi)$  which are constant along each flow line. The metric can be written in the form

$$\begin{aligned} ds^2 &= e^{2\nu} dt^2 - e^{2\lambda} dr^2 - R^2 d\Omega^2, \\ d\Omega^2 &= d\theta^2 + \sin^2 \theta d\phi^2, \end{aligned} \quad (2)$$

where  $\nu$ ,  $\lambda$  and  $R$  are functions of  $r$  and  $t$ . The equations have a first integral,  $m(r, t)$ , which can be interpreted as the mass within comoving radius  $r$  at time  $t$ . Unless  $\alpha = 0$ , this first integral decreases with increasing  $t$  because of the work done by the pressure. Spherically symmetric self-similar solutions can be put into a form in which

all dimensionless quantities, such as  $\nu$ ,  $\lambda$ ,  $S \equiv R/r$ ,  $\mu t^2$  and  $M \equiv m/R$ , are functions only of the dimensionless self-similar variable  $z = r/t$  [1]. Varying  $z$  for a given  $t$  specifies the spatial profile of various quantities. For a given value of  $r$  (i.e., for a given fluid element), it specifies their time evolution.

Some of these quantities have a particularly straightforward physical interpretation. Thus  $S$  is the scale factor,  $\mu t^2$  specifies the density profile at time  $t$  and the mass function  $M$  is related to the divergence of the congruence of outgoing null geodesics. Values of  $z$  for which  $M = \frac{1}{2}$  correspond to a black hole or cosmological apparent horizon since this divergence is zero. Another important quantity is the function

$$V(z) = e^{\lambda - \nu} z, \quad (3)$$

which represents the velocity of the spheres of constant  $z$  relative to the fluid. This should not be confused with the velocity of the fluid with respect to a Schwarzschild foliation, the ‘radial 3-velocity’, which we denote by  $V_R$ . Special significance is attached to values of  $z$  for which  $|V| = \sqrt{\alpha}$  and  $|V| = 1$ . The first corresponds to a sonic point, the second to a black-hole event horizon or a cosmological particle horizon.

It is convenient to introduce a dimensionless function  $x(z)$  defined by

$$x(z) \equiv (4\pi\mu r^2)^{-\alpha/(1+\alpha)}. \quad (4)$$

The conservation equations  $T^{\mu\nu}_{;\nu} = 0$  can then be integrated to give

$$e^\nu = \beta x z^{2\alpha/(1+\alpha)}, \quad e^{-\lambda} = \gamma x^{-1/\alpha} S^2, \quad (5)$$

where  $\beta$  and  $\gamma$  are integration constants. The remaining field equations reduce to a set of ordinary differential equations in  $x$  and  $S$  (given explicitly in Appendix A.1). Thus, the governing equations in the comoving approach consist of an effectively 2-dimensional system of non-autonomous ordinary differential equations. However, it is also useful to regard the solutions as trajectories in the 3-dimensional  $(x, S, \dot{S})$  space (where a dot denotes  $z d/dz$ ). Each trajectory is parametrized by the similarity variable  $z$ , so there is a 2-parameter family of spherically symmetric self-similar solutions for a given equation-of-state parameter  $\alpha$ . Note that  $z$  may be either positive or negative but it always has the same sign as  $V$ .

There is considerable arbitrariness in the selection of the axes that specify the solution space: although CC take them to be  $S$ ,  $\dot{S}$  and  $x$ , Foglizzo & Henriksen ([12]; FH) take them to be  $\mu$ ,  $V$  and a variable linearly related to  $\dot{S}$ . In either case, the functions have an obvious physical significance. The comoving approach thus has considerable intuitive appeal in that it affords immediate physical insights. For example, one can write down the metric explicitly and see immediately where the density goes infinite and the singularities occur.

One disadvantage of the comoving approach is that the similarity variable  $z$  can be badly behaved. For example, sometimes finite values of  $z$  correspond to zero or infinite physical distances from the origin and sometimes zero values of  $z$  correspond to non-zero distances. Also many solutions span both negative and positive values of  $z$ , which means that  $z$  must jump from  $+\infty$  to  $-\infty$ . FH avoid this problem by using the coordinate  $\xi \equiv 1/z$  but they then have a discontinuity at  $z = 0$ . Another disadvantage is that the comoving approach, at least with the variables used by CC and FH, makes rigorous proofs of general features of SSS solutions difficult.

In  $(x, S, \dot{S})$  space the sonic condition  $|V| = \sqrt{\alpha}$  specifies a 2-dimensional surface. Where a curve intersects this surface, the equations do not uniquely determine  $\dot{x}$  (i.e.,

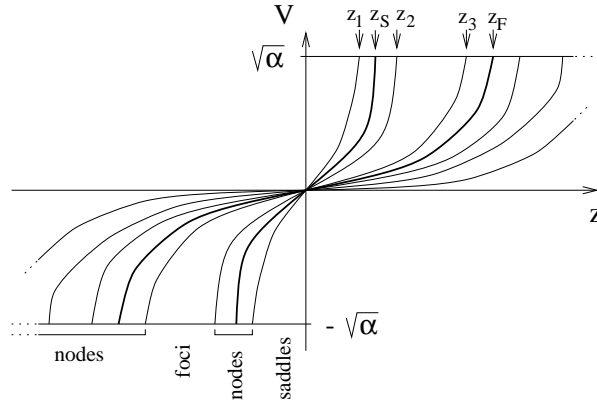


**Figure 1.** The different regions of the sonic line  $Q$  in terms of a  $V(z)$  diagram. Note that there exist two sonic lines with  $V = \pm\sqrt{\alpha}$ . The curves represent the subsonic parts ( $|V| < \sqrt{\alpha}$ ) of some solutions with a regular centre (to be discussed in more detail below). In addition, the static solution has been included. The thick curves correspond to the flat Friedmann solution and the static solution. Note that the orbits in one quadrant constitute the time-reverses of the orbits in the other quadrant. Thus, for example, the expanding Friedmann solution appears in the upper-right quadrant, while the contracting Friedmann solution is depicted in the lower-left quadrant.

the pressure gradient), so there can be a number of different solutions passing through the same point. However, only integral curves which pass through a line  $Q$  on the sonic surface, the *sonic line*, are ‘regular’ in the sense that they can be extended beyond there. Thus the sonic surface ‘filters out’ the small subset of solutions that are physical. The behaviour near the sonic line can be treated as an eigenvalue problem [2, 11]. It can be shown that the equations permit just two values of  $\dot{x}$  at each point of  $Q$  and there will then be two corresponding values of  $\dot{V}$  [13]. If the values of  $\dot{V}$  are complex, corresponding to a *focal* point, then the solution will still be unphysical. If they are real, at least one of the values of  $\dot{V}$  must be positive. If both values of  $\dot{V}$  are positive, corresponding to a *nodal* point, the smaller value is associated with a 1-parameter family of solutions, while the larger one is associated with an isolated solution. The eigenvector direction associated with the 1-parameter set is referred to as *dominant* or *primary* and the other direction as *secondary*. If one of the values of  $\dot{V}$  is negative, corresponding to a *saddle* point, both values are associated with isolated solutions.

On each side of a sonic point,  $\dot{x}$  may have either of the two values. If one chooses different values for  $\dot{x}$ , there will be a discontinuity in the density, pressure and velocity gradients. If one chooses the same value, there may still be a discontinuity in the higher derivatives of  $x$ . Only the isolated solution and a single member of the 1-parameter family of solutions are analytic (or at least  $C^\infty$ ) and these are associated with the two eigenvector directions. One can show that the part of  $Q$  for which there is a 1-parameter family of solutions corresponds to two ranges of values for  $z$  for each sign of  $z$ . One range ( $z_1 < |z| < z_2$ ) lies to the left of the Friedmann sonic point  $z_F$  and includes the static sonic point  $z_S$ ; the other range ( $|z| > z_3$ ) includes the Friedmann sonic point. These features are illustrated in figure 1. When  $\alpha = \frac{1}{3}$ , it happens that  $z_2 = z_S$  and  $z_3 = z_F$ .

CC have classified the  $p = \alpha\mu$  SSS solutions in terms of their asymptotic

behaviour. The key steps in their analysis are: (1) a complete analysis of the dust ( $\alpha = 0$ ) solutions, since this provides a qualitative understanding of some of the solutions with pressure in the supersonic ( $|V| > \sqrt{\alpha}$ ) regime; (2) an elucidation of the link between the  $z > 0$  and  $z < 0$  solutions; (3) a proof that, at large and small values of  $|z|$ , all self-similar solutions must have an asymptotic form in which  $x$  and  $S$  have a power-law dependence on  $z$ ; and (4) a demonstration that there are only three *exact* power-law solutions – the flat Friedmann model, a self-similar static model and a self-similar Kantowski-Sachs model. Prompted by results obtained by GNU, CC also find: (5) a family of power-law solutions which are ‘asymptotically Minkowski’ at large  $|z|$ ; and (6) a family of solutions which are ‘asymptotically Minkowski’ at a *finite* value of  $z$  and which have a power-law dependence on  $\ln z$ . These new solutions only exist for  $\alpha > 1/5$ ; they were missed in CC’s original analysis but they were then able to extend their work to include them.

## 2.2. The homothetic approach

When the homothetic Killing vector is non-null, the line element adapted to the homothetic vector field can be written in a diagonal form [2]

$$ds^2 = \begin{cases} e^{2X} d\hat{s}^2 = e^{2X} [dT^2 - D_1^2(T)dX^2 - D_2^2(T)d\Omega^2] \\ e^{2T} d\bar{s}^2 = e^{2T} [D_1^2(X)dT^2 - dX^2 - D_2^2(X)d\Omega^2] \end{cases}, \quad (6)$$

where we have distinguished between when the homothetic vector field is spacelike ( $\partial/\partial X$ ; upper line element) and when it is timelike ( $\partial/\partial T$ ; lower line element). The unphysical spacetimes,  $d\hat{s}^2$  and  $d\bar{s}^2$  respectively, are hypersurface homogeneous [14, 15] and the approach used by GNU exploits similarities with the equations governing spatially homogeneous models (see, e.g., [16]).

By demanding that the energy density be non-negative, dominant quantities can be determined, and bounded dimensionless variables are obtained separately for the spatially and the timelike SSS regions. In each of the two cases, a suitable dimensionless independent variable is chosen, so that only one dependent variable has dimensions. Using these variables, Einstein’s equations and the conservation equation  $T^{\mu\nu}{}_{;\nu} = 0$  result in a dynamical system in which the equation for the dimensionful variable is decoupled. The remaining equations form 4-dimensional autonomous dynamical systems, where the dynamical variables are related by a constraint (see Appendix A.2). One of the variables is  $V$ , defined in the comoving context above. It is related to the tilt of the fluid flow with respect to the homothetic symmetry surfaces.

Since GNU introduce four bounded variables, locally related by a constraint (for similar treatments, see [17, 18]), solutions are effectively treated as orbits in a compact 3-dimensional state space. The fact that the state space can be compactified is of great advantage in that one can visualize all the solutions at a glance and this will be exploited throughout this paper. However, the physical interpretation may still be difficult. For example, parts of the boundary of the state space are not always themselves self-similar, as exemplified by the non-self-similar Kantowski-Sachs state space that appears as a boundary submanifold of the spatially SSS state space.

The study of the self-similar spherically symmetric solutions now corresponds to studying the orbits in the state space of these dynamical systems. The future and past asymptotes of the orbits are important for understanding the corresponding models and are associated with equilibrium points in the state space. Indeed, there

**Table 1.** Interpretation of solutions asymptotic to the given equilibrium points.

Label	Interpretation
C	Solutions with a regular centre or infinitely dispersed solutions.
M, $\tilde{M}$	‘Asymptotically Minkowski’ solutions.
K	Non-isotropic singularity solutions.
F	Asymptotically Friedmann (isotropic singularity) solutions.
T	Exact static solution.

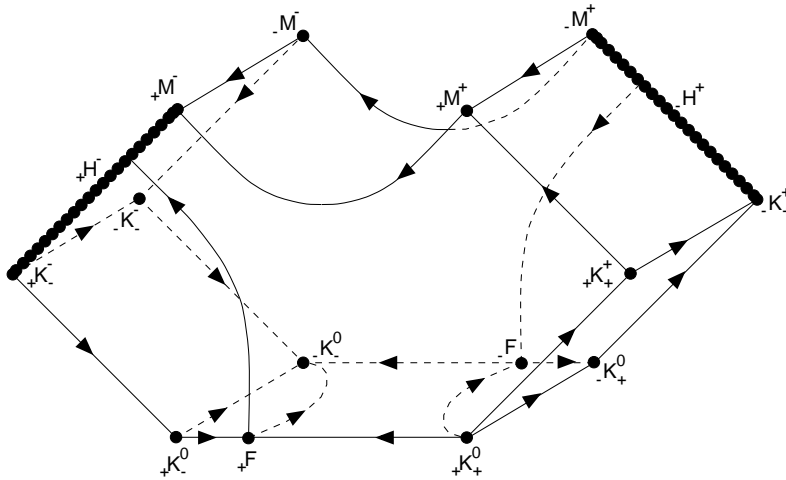


**Figure 2.** The spatially SSS reduced state space for  $\alpha \leq \frac{1}{5}$ . For more details, see GNU1.

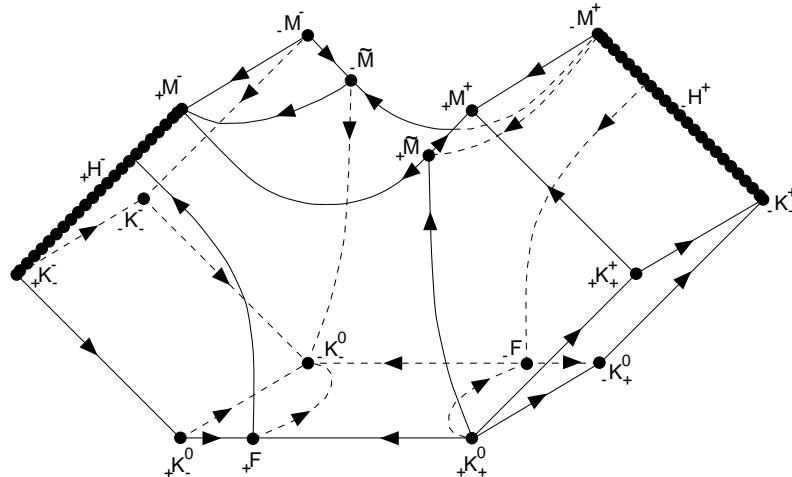


**Figure 3.** The spatially SSS reduced state space for  $\alpha > \frac{1}{5}$ . Note that the equilibrium points  $\pm\tilde{M}$  now have entered the spatially SSS state space.

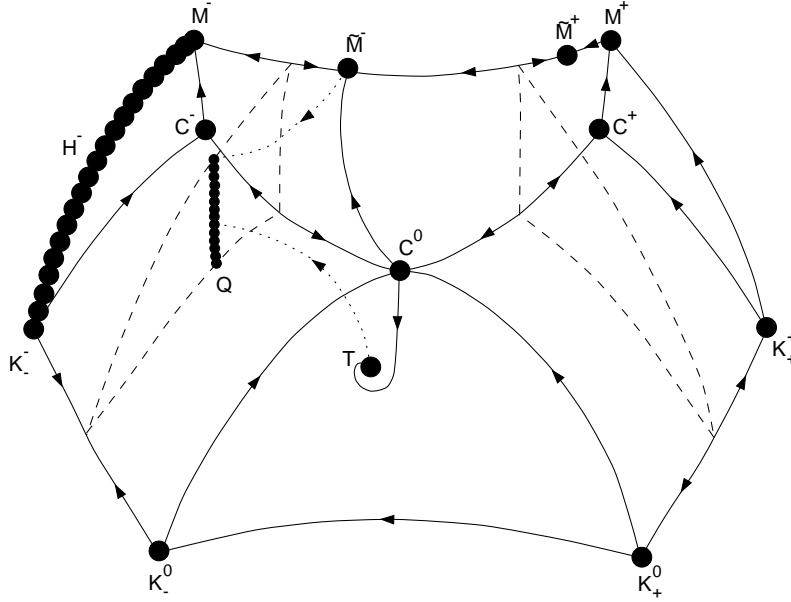


**Figure 4.** The timelike SSS reduced state space for  $\alpha < \frac{1}{5}$ . The dashed curves indicate the boundaries of the sonic surfaces, located at  $V = \pm\sqrt{\alpha}$ . The bulleted line in one of these surfaces is the sonic line  $Q$ . For more details, see GNU2.

is a simple correspondence between these points and the asymptotic classification of CC, as discussed in sections 2.3 and 3. Such points correspond to solutions with higher symmetry and always lie on the boundary of the state space. They often have a straightforward interpretation. The M points, for example, correspond to the Minkowski solution with a certain slicing. Here we will be interested in solutions asymptotic to the various equilibrium points, rather than the points themselves. Thus solutions asymptotic to the M points are ‘asymptotically Minkowski’ and those associated with F are asymptotic to the flat Friedmann solution. The interpretations of different asymptotes are summarized in table 1.

The labels used for the equilibrium points are sometimes accompanied by subscripts and/or superscripts referring to the values of some of the dynamical variables at that point. Note that models corresponding to an equilibrium point in a spatially homogeneous slicing, such as the flat Friedmann model, will correspond to orbits in state space in a slicing associated with the homothety. An orbit in state space describes a particular solution, each point on the orbit giving the solution on a particular homothetic slice (up to a scale factor, which is determined by the decoupled ‘scale’ equation).

Equilibrium points and flows along eigenvector directions for the spatially SSS reduced state space are depicted in figures 2 and 3. There is a monotonic function for this system when  $|V^{-1}| > 0$  (GNU1). As there are no invariant submanifolds with  $V^{-1} = 0$  in the interior, all equilibrium points lie on the boundary of the state space. Equilibrium points and flows along eigenvector directions for the timelike SSS reduced state space are depicted in figures 4 and 5. As for the spatially SSS region, there is a monotonic function of the timelike SSS state space when  $|V| > 0$  unless  $|V| = \sqrt{\alpha}$  [3].

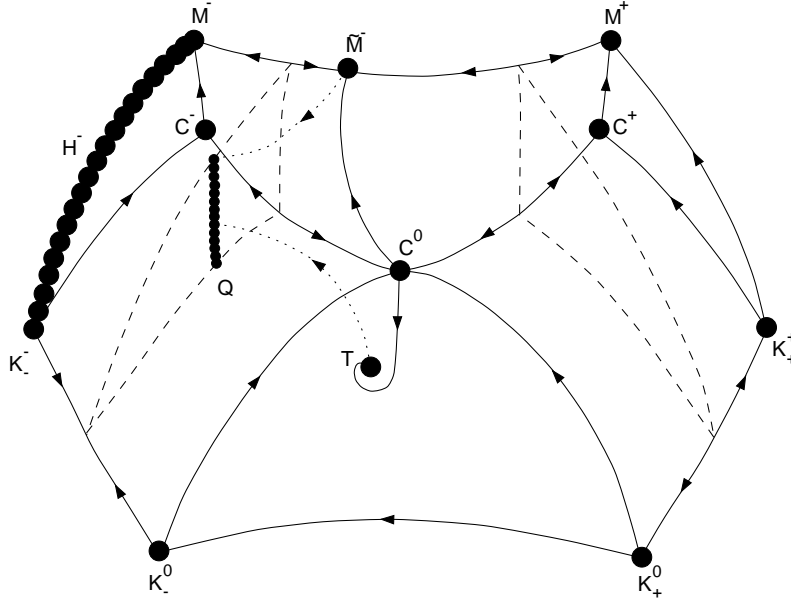


**Figure 5.** The timelike SSS reduced state space for  $\alpha \geq \frac{1}{5}$ . Note that the equilibrium point  $\tilde{M}^+$  now has left the timelike SSS state space.

The sonic surfaces are located at  $|V| = \sqrt{\alpha}$  in the timelike SSS regions, see figures 4 and 5. As discussed in section 2.1, solutions must cross the sonic surface on the sonic line  $Q$  in order to be regular. Such a sonic line is only present in one of the sonic surfaces. This, together with the fact that there is a monotonic function for  $|V| > 0$ , implies that solutions entering the other half of the state space (the right half of figures 4 and 5) are unphysical (see GNU2). In addition, all orbits in the right half of figure 4 (figure 5) pass through a sonic surface and end at the sink  $\tilde{M}^+$  ( $M^+$ ), so that all these solutions have an irregular sonic point. It also turns out that solutions there have negative mass.

In order to obtain a fully global picture of the solution space, the state spaces of the spatially and the timelike SSS regions must be matched. This is done at equilibrium points for which  $|V| = 1$ . The change of causality of the symmetry surfaces there corresponds to a Cauchy horizon in these variables. In figure 6, the spatially SSS state space has been matched with two timelike SSS state spaces along the lines of equilibrium points  $H$ . These lines of equilibrium points are artifacts of the homothetic approach and appear because the coordinates break down when  $|V| = 1$ . Thus, the state space is ‘pinched off’ there, as seen in the figure. When matching, one must adjust the directions of the state space flows in the regions. For example, when following orbits from the timelike SSS region into the spatially SSS region via  ${}_+H^-$ , the state space flow in the spatially SSS region will be opposite to that of figures 2 and 3. One of the matchings is done for  $V = +1$ . The sonic line of the corresponding timelike SSS state space will then be located in the sonic surface at  $V = +\sqrt{\alpha}$ . Consequently, due to the monotonic function discussed above,  $V < 0$  is an unphysical region in this state space. The other timelike SSS state space is attached where  $V = -1$ . In that state space, the sonic line will be located at  $V = -\sqrt{\alpha}$ , and  $V > 0$  is an unphysical



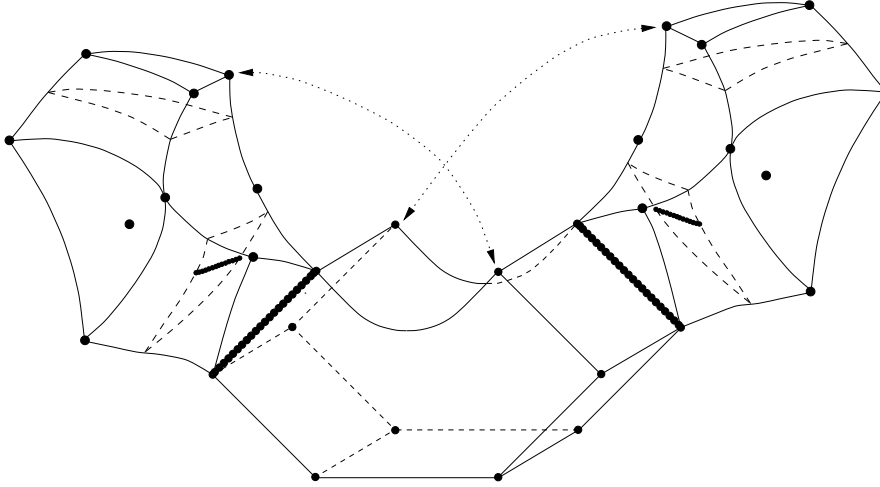


**Figure 6.** Matching the spatially SSS region with two timelike SSS regions. Note that the equilibrium points  $\pm M^\pm$  are matched with  $M^+$  in each of the timelike SSS regions, as indicated by the dotted arrows.

**Table 2.** Possible initial and final equilibrium points of orbits in the matched state space, together with the number of parameters necessary to describe the solutions near a certain equilibrium point.

Parameters	Sink/source 2	Separatrix-generating 1	One orbit –
$\alpha \leq \frac{1}{5}$	$\pm K_\pm^0, (\tilde{M}^+)$	$\pm F, C^0$	T
$\alpha > \frac{1}{5}$	$\pm K_\pm^0, \pm M^\pm$	$\pm F, C^0, \pm \tilde{M}$	T

region.

The possible initial and final equilibrium points of orbits are the following (see table 2): for  $\alpha \leq \frac{1}{5}$  (see figures 2 and 4), the only equilibrium points that are sources or sinks are  $\pm K_\pm^0$  in the spacelike SSS region and  $\tilde{M}^+$  in each timelike SSS region. Note that the points  $\tilde{M}^+$  are located in the unphysical part of each timelike SSS region. In addition,  $\pm F$  and  $C^0$  are separatrix-generating equilibrium points, i.e., points for which there is a 1-parameter set of orbits, spanning a surface in the interior of the state space. The static solution is represented both by the equilibrium point T and by an orbit through the interior of the timelike and spatially SSS state spaces. This orbit is the only interior orbit connected with T. When  $\alpha > \frac{1}{5}$ , the equilibrium points  $\pm M^\pm$  change stability from saddles and become sinks or sources. In addition, the separatrix-generating points  $\pm \tilde{M}$  appear in the spatially SSS state space (see figure 3). No new features appear in the left-hand parts of figures 4 and 5, i.e., the parts of the timelike SSS state space associated with physically interesting solutions.

### 2.3. Comparison between the two approaches

It should be stressed that some of the differences between the two approaches are not intrinsic but merely reflect the particular realizations used by CC and GNU.

For example, one could in principle use compactified variables in the comoving approach and one could also express solutions in terms of the similarity variable in the homothetic approach. Indeed the variables used to represent the solutions in the two approaches must always be mathematically related in some way (except in spacetime regions where one or both sets of coordinates break down). However, since the coordinate descriptions of the spacetime are very different, physical comparison is non-trivial. Also, each approach suggests different ‘natural’ dependent and independent variables, so variables found in one approach can be difficult to express in the other.

CC emphasize the behaviour of solutions in the asymptotic limit  $|z| \rightarrow \infty$ , since the behaviour of solutions in this limit can only take one of a few simple forms (asymptotically Friedmann, asymptotically Kantowski-Sachs, and what they term asymptotically ‘quasi-static’). However, the limit  $|z| \rightarrow \infty$  does not usually play a crucial role in the GNU analysis but just corresponds to some region of their state space. In particular, there is no equilibrium point corresponding to CC’s asymptotically quasi-static solutions since  $|z| \rightarrow \infty$  in this case corresponds to a surface *within* the state space. CC also discuss the behaviour of solutions in the limit  $z \rightarrow 0$  and find that the solutions are either exactly static or asymptotically Friedmann at the origin.

CC place considerable emphasis on the form of the velocity function  $V(z)$ . This is useful if one wishes to identify event horizons, sonic points and physical singularities. (In the GNU analysis these conditions correspond respectively to the lines H, the surfaces  $|V| = \sqrt{\alpha}$  and the equilibrium points K.) However, it must be emphasized that the  $V(z)$  representation alone yields an incomplete understanding of solutions since one is projecting them onto a particular 2-dimensional plane, so that many physically distinct solutions may be superposed. For example, only in the  $\alpha = \frac{1}{3}$  (radiation) case does the region of the 3-dimensional solution space in which the mass is negative correspond to a well-defined region of  $V(z)$  space; otherwise it depends on the third axis. CC also emphasize the form of the scale factor  $S(z)$  and the mass function  $M(z)$ . These quantities provide important physical insights into the solutions but one should bear in mind that they only represent different 2-dimensional projections of the full 3-dimensional state space.

In the homothetic approach, the variables are chosen for their mathematical properties. This makes it possible to obtain a compact state space, and thus a complete visual picture of the solution space. The homothetic formulation also provides rigorous proofs and enables one to use the insights gained from Bogoyavlensky’s analysis [2]. On the other hand, this approach is rather technical, and one can only indirectly gain physical insights.

A complication in the diagonal homothetic approach is that the spacetime must be covered by several coordinate patches, since the coordinates break down when the homothetic Killing vector becomes null,  $|V| = 1$  (see section 2.2). This is physically equivalent to when the fluid 4-velocity becomes null. Since many SSS solutions cross  $|V| = 1$ , one is forced to consider the relationship to other approaches if one wants to understand the global nature of each solution. Thus, in order to investigate when and exactly how orbits pass from one regime to the other (e.g., timelike to spacelike) in the homothetic approach, the dynamics are considered in the comoving approach. Going back and forth between the homothetic and comoving approaches leads to a complete understanding of the dynamics across the null surface and allows a check of the internal consistency of both approaches. This is another illustration of how the two approaches are complementary and how it is only by using the two approaches in

tandem that a full understanding is achieved.

Variable and coordinate transformations can be used to relate the comoving and homothetic variables explicitly (see GNU1, GNU2 [4, 5]), although care must be taken in effecting these transformations, and it should be noted that there are some typographical errors in Appendix B of GNU1. An alternative and perhaps a more elegant procedure is to use expressions for dimensionless quantities, such as  $\mu t^2$  and  $2m/R$ , in each approach. Together with the covariant expression for  $V$ , given by Cahill and Taub [1] (see equation A.18), it is straightforward to use these to relate the variables of the two approaches.

#### 2.4. The Schwarzschild approach

We should also mention the ‘Schwarzschild’ approach. This is useful when matching a self-similar interior region to an asymptotically flat (non-self-similar) exterior region. Schwarzschild coordinates are also useful if one wishes to solve the equations of motion for the null geodesics, as required in studying the global structure of the solutions. Consequently it was used by OP to study naked singularities and the cosmic censorship hypothesis in the context of SSS solutions. However, the disadvantage of Schwarzschild coordinates is that they involve non-physical singularities (see [2], pp. 158–159). The transformations between comoving and Schwarzschild coordinates are given explicitly by OP.

### 3. Solutions and their physical interpretation

In this section, we discuss various types of solutions and their physical properties. The strategy will be to depict a given solution class in state space but – in order to extract physical features – to also plot the following physical quantities as functions of  $z$ : the scale factor  $S$ ; the velocity function  $V$ ; the density profile  $\mu t^2$ ; and the mass function  $2m/R$  ( $= 2M$ ). Another quantity of physical interest is the asymptotic energy per unit mass  $E$  and this will be useful in parametrizing solutions. The expressions for these quantities are collected in Appendix A.3.

#### 3.1. General solution structure

Solutions can be classified by considering their global features, as well as their asymptotic properties. One possibility is to consider their differentiability. Another is to use the global causal properties of the homothetic Killing vector  $\eta^\alpha$  and we now consider this. (1) There are solutions for which  $\eta^\alpha$  is purely timelike; these develop a shock, since their orbits necessarily end at an irregular sonic point. (2) There are solutions for which  $\eta^\alpha$  always is spacelike; these always have  $|V| > 1$ . (3) There are also solutions, such as the flat Friedmann solution, for which  $\eta^\alpha$  changes causality once. (4) Solutions with two causality changes include, for example, the static solution and some asymptotically Friedmann solutions that recollapse. (5) Solutions that undergo three changes of the causality include those that develop a naked singularity. For more examples, see table 3. We will now discuss some specific examples in more detail.

#### 3.2. Asymptotically Friedmann solutions

There are two distinct 1-parameter families of asymptotically Friedmann solutions as  $|z| \rightarrow \infty$ , one with  $z > 0$  and the other with  $z < 0$ . The parameter characterizing

**Table 3.** Classification of orbits. T and S stand for timelike and spacelike, respectively.

Causality	Example
T	Solutions with an irregular sonic point.
S	Recollapsing asymptotically Friedmann solutions, always having $ V  > 1$ . Recollapsing asymptotically quasi-static solutions, always having $ V  > 1$ .
TS	Asymptotically Friedmann solutions that expand forever, including the flat Friedmann solution itself. Asymptotically quasi-static solutions that collapse to form a black hole.
TST	The static solution.
STS	Asymptotically Friedmann solutions that recollapse but have $ V  < 1$ for part of their evolution. Asymptotically quasi-static solutions that expand and recollapse, having $ V  < 1$ for part of the evolution; these can also be of type STSTS.
TSTS	Asymptotically quasi-static solutions that collapse to form naked singularities.

these solutions measures the underdensity or overdensity relative to the flat Friedmann solution and is also associated with the asymptotic energy  $E$ . In terms of the GNU state space, the asymptotically Friedmann solutions start at the F equilibrium points in the spatially SSS region (see figure 7, where one of the two equivalent families of the asymptotically Friedmann solutions is depicted). Physically interesting quantities are illustrated in figure 8. The  $z > 0$  solutions correspond to inhomogeneous models that start from an initial Big Bang singularity at  $z = \infty$  ( $t = 0$ ) and then, as  $z$  decreases, either expand to infinity or recollapse. The  $z < 0$  solutions are just the time-reverse of these. Depending on the value of  $E$ , two qualitatively different types of solutions can be distinguished:

1) For solutions that are sufficiently overdense with respect to the flat Friedmann solution (i.e., for  $E$  less than some critical negative value  $E_{\text{crit}}$ ),  $|V|$  reaches a minimum and then rises again to infinity as  $|z|$  decreases, indicating the formation of a non-isotropic singularity at which  $S \rightarrow 0$  for finite a value of  $z$ . The solutions in this class are of type S or STS in the classification of section 3.1. Such solutions correspond to black holes growing at the same rate as the Universe [19, 20, 11, 21]. They are represented by dotted curves in figures 7 and 8. Providing the minimum of  $|V|$  is below 1, there is a black-hole event horizon and a cosmological particle horizon where  $|V| = 1$ . Otherwise the entire Universe is inside the black hole, although there is always an apparent horizon since CC show that the minimum of  $M$  is necessarily below  $1/2$ .

2) All solutions which are underdense or not sufficiently overdense ( $E > E_{\text{crit}}$ ) reach the sonic surface at  $|V| = \sqrt{\alpha}$ . The solutions in this class are of type TS in the classification of section 3.1. Those which reach the sonic line Q, and in addition have  $z_1 < |z| < z_2$  or  $|z| > z_3$  at the sonic point (see figure 1), may be attached to the origin

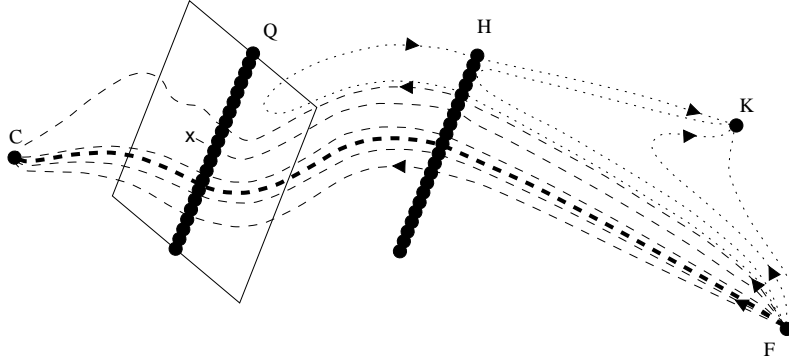


**Figure 7.** Asymptotically Friedmann solutions as orbits in state space. Recollapsing solutions are represented by dotted curves. Also shown are solutions that reach the sonic surface (dashed curves), some of which can be continued to a dispersed state C. The continuations are exemplified by solutions with no oscillation in  $V_R$  (four curves) and one oscillation in  $V_R$  (one curve). The flat Friedmann solution is indicated by the thick dashed curve. 'x' marks an irregular sonic point.

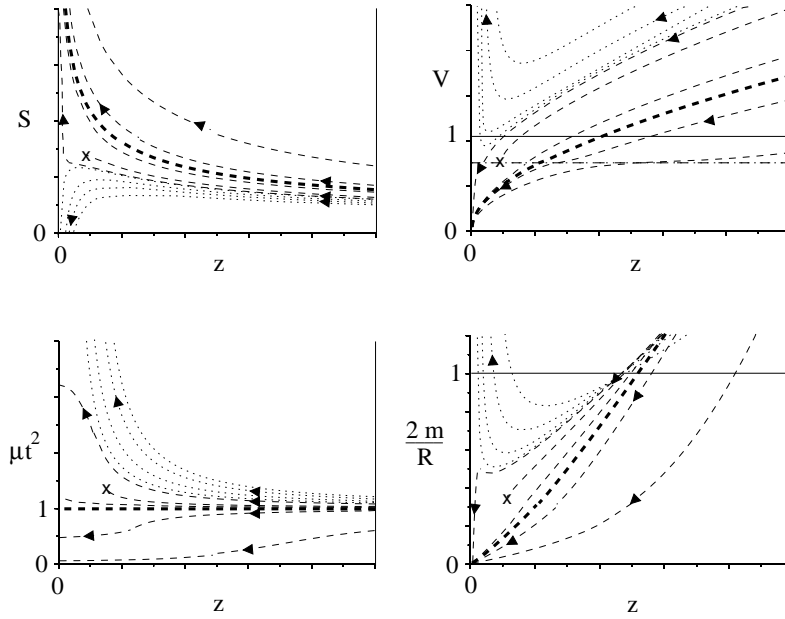


**Figure 8.** Physical quantities for the asymptotically Friedmann solutions. The dash-dotted line in the  $V(z)$  diagram corresponds to the sonic surface. Other designations are given in the caption of figure 7. The  $\mu t^2$  diagram has been normalized so that the flat Friedmann solution corresponds to  $\mu t^2 = 1$ . The relation to the state space is as follows: the Friedmann point F corresponds to  $z \rightarrow \infty$ ; the non-isotropic singularity (K) corresponds to  $S \rightarrow 0$  for finite values of  $z$  (dotted curves only); orbits reaching  $z = 0$  correspond to infinitely dispersed solutions (the point C; dashed curves only).

by subsonic ( $|V| < \sqrt{\alpha}$ ) solutions. In figures 7 and 8, these asymptotically Friedmann solutions are represented by dashed curves. Subsonic continuations that have a regular centre have been included whenever possible. The solutions with a regular centre are also described by a single parameter and this is a measure of the density at the origin  $z = 0$ . These transonic solutions represent density fluctuations that grow at the same rate as the particle horizon [13]. Numerical calculations indicate that these solutions can generally only be matched to the centre non-analytically. While there is a continuum of regular underdense solutions, regular overdense solutions only occur in narrow bands (with just one solution per band being analytic). The overdense solutions exhibit oscillations in the subsonic region, with the number of oscillations labeling the band. Solutions with larger number of oscillations form ever narrower bands within the one-oscillation band (in terms of the ranges of  $z$  at Q). The existence of these subsonic bands was first pointed out by Bogoyavlensky [2] and also studied by Ori & Piran [9], Carr & Yahil [13] and GNU2. The higher bands are all nearly static near the sonic point ( $z \approx z_S$ ), although they deviate from the static solution and approach the equilibrium point C as  $z \rightarrow 0$ .

### 3.3. Asymptotically quasi-static solutions

As discussed by CC, there is exactly one self-similar static solution for each value of  $\alpha$ , a 1-parameter family of solutions that are asymptotically static (in the sense that the radial 3-velocity  $V_R$  tends to zero as  $|z| \rightarrow \infty$ ) and a 2-parameter family of solutions that are asymptotically ‘quasi-static’ (in the sense that  $\dot{S} \rightarrow 0$  but  $V_R$  is finite). One of these parameters can be taken to be the asymptotic energy  $E$ , while the other (denoted by  $D$ ) can be related to the value of  $z$  at the Big Bang or Big Crunch singularity. It should be emphasized that the solutions in this class may only be close to the static solution for part of their evolution. For example, the class includes expanding models that finally recollapse. This is clearly illustrated by some of the state-space orbits in figure 9.

The key feature of these solutions is that they span both negative and positive values of  $z$ . Whereas the asymptotically Friedmann solutions are confined to  $z > 0$  or  $z < 0$  and are symmetric in  $z$  (changing the sign of  $z$  just reverses the time direction), the asymptotically quasi-static solutions are in general asymmetric in  $z$  and necessarily pass from  $z = -\infty$  to  $z = +\infty$ . This is because the Big Bang occurs at  $z = -1/D$  (corresponding to a non-zero value of  $t$ ) in these solutions, so the limit  $|z| \rightarrow \infty$  has no particular physical significance. They can be interpreted as inhomogeneous cosmological models with an advanced Big Bang. Equivalently, for the time-reversed solutions, there is a Big Crunch singularity at  $z = +1/D$ . As illustrated in figures 9 and 10, there are two types of asymptotically quasi-static solutions:

1) Expanding and recollapsing solutions. Solutions with  $E$  less than some critical negative value  $E_{\text{crit}}(D)$  expand from an initial singularity in the  $z < 0$  region and then recollapse to another singularity in the  $z > 0$  region. In terms of the classification of section 3.1, these are of type S, STS or STSTS. The value of  $z$  is  $-1/D$  at the initial singularity but depends on both  $E$  and  $D$  at the final one. These solutions are represented by dotted curves in figures 9 and 10. As  $z$  decreases from  $-1/D$ ,  $V$  rises from  $-\infty$ , reaches a maximum below  $-\sqrt{\alpha}$  but possibly above  $-1$  and then tends to the quasi-static form as  $z \rightarrow -\infty$ . The solution then jumps to  $z = +\infty$  and enters the  $z > 0$  regime. As  $z$  continues to decrease,  $V$  decreases to a minimum above  $\sqrt{\alpha}$  and then tends to  $+\infty$  at the value of  $z$  corresponding to the recollapse singularity.

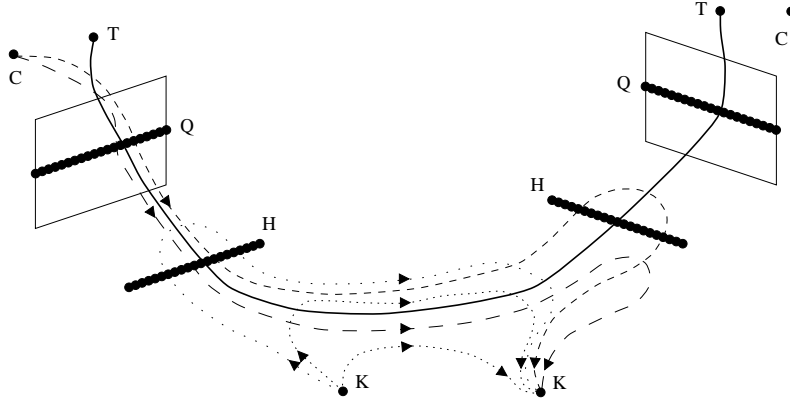


**Figure 9.** Asymptotically quasi-static solutions as orbits in state space. Dotted curves correspond to recollapsing solutions, while dashed curves correspond to ever-collapsing solutions. In particular, the short-dashed curve corresponds to a solution having a naked singularity. Note that there also are solutions of the ever-expanding type. These go from the left-most K-point to the right-most C-point, in analogy with the ever-collapsing ones displayed here. The heavy full curve corresponds to the static solution.  $V$  and  $z$  are negative in the left half of the state space, and positive in the right half.

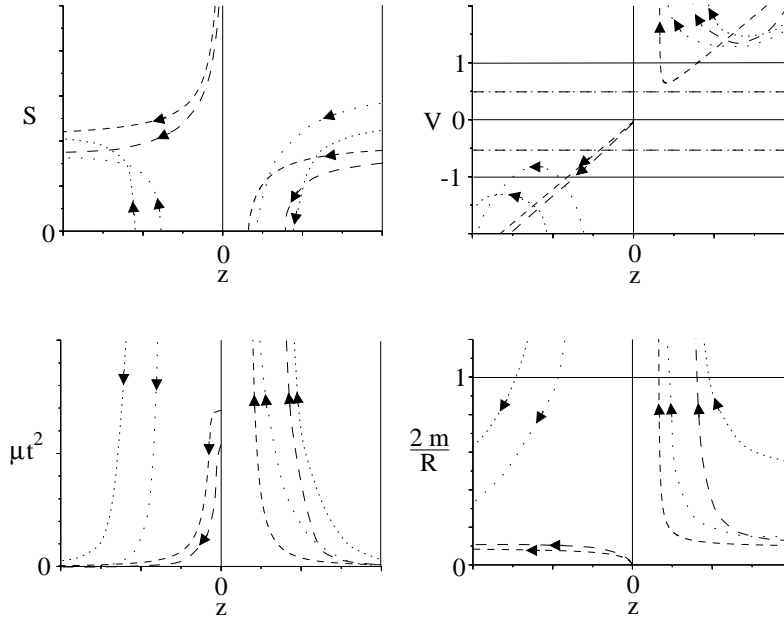


**Figure 10.** Physical quantities for asymptotically quasi-static solutions. The dash-dotted lines in the  $V(z)$  diagram correspond to the sonic lines. Other designations are given in the caption of figure 9. The relation to the state space is as follows:  $S \rightarrow 0$ ,  $\mu t^2 \rightarrow \infty$ ,  $2m/R \rightarrow \infty$  correspond to non-isotropic singularities (K points);  $S \rightarrow \infty$ ,  $V \rightarrow 0$ ,  $\mu t^2$  finite,  $2m/R \rightarrow 0$  correspond to infinitely dispersed solutions (C points; dashed curves only). Note that  $|V| \rightarrow \infty$  both at the points K and when  $z$  jumps from  $-\infty$  to  $\infty$ , the latter case corresponding to a surface cutting the state space into two halves.

If the minimum of  $V$  is below 1, one necessarily has a black-hole event horizon and a cosmological particle horizon; this occurs if  $E$  exceeds some negative value  $E_*(D)$ . The minimum of  $V$  will reach  $\sqrt{\alpha}$  when  $E$  reaches  $E_{\text{crit}}(D)$  and this corresponds to the last recollapsing solution. One also has the time-reverse of these solutions.

The solutions with  $E > E_{\text{crit}}(D)$  are of two types:

2a) Ever-collapsing solutions. These start out from an infinitely dispersed state and describe the collapse of an inhomogeneous gas cloud to a non-isotropic singularity at  $z = +1/D$  (i.e., after  $t = 0$ ). In terms of the classification of section 3.1, these are of type TS or TSTS. The dashed curves in figures 9 and 10 correspond to these solutions. They start at the point C with  $V = 0$  at  $z = 0$  and then, as  $z$  decreases, reach a sonic point where  $V = -\sqrt{\alpha}$ . The solution is then attached to a supersonic asymptotically quasi-static solution at the sonic line. In this context, it should be noted that the introduction of the ‘second’ parameter  $D$  has relatively little effect on the form of the solutions in the subsonic regime. Indeed, one can show that all solutions apart from the exactly static solution must be asymptotic to the flat Friedmann solution at small  $|z|$ . In particular, the models can collapse from infinity (i.e.,  $S \rightarrow \infty$  as  $z \rightarrow 0$  or  $t \rightarrow -\infty$ ) only if  $E$  is positive or lies in discrete bands if negative. The supersonic solutions pass through a Cauchy horizon (where  $V = -1$ ) before tending to the quasi-static form at  $z = -\infty$  and jumping to  $z = +\infty$ . The continued evolution for  $z > 0$  resembles the evolution of case (1): as  $z$  further decreases,  $V$  first reaches a minimum and then diverges to infinity when it encounters the singularity at  $z = 1/D$ . The minimum will be below 1 if  $E$  is less than some negative value  $E_+(D)$ , and in this case one necessarily has a naked singularity, as pointed out by OP. Particular examples of this are some of the general-relativistic Penston-Larson solutions (see figure 13 of OP). That  $D$  has different values for different solutions is clearly seen in the  $S(z)$  graph in figure 10.

2b) Ever-expanding solutions. These are the time reverse of the ever-collapsing solutions. They resemble case (1) in the  $z < 0$  regime but take a different form after they have passed into the  $z > 0$  regime. As  $z$  decreases from  $+\infty$ ,  $V$  (rather than reaching a minimum) decreases monotonically until it encounters a sonic point at  $V = \sqrt{\alpha}$ . If this sonic point is located in the physical ranges of the sonic line Q, the solution may be attached to the origin  $z = 0$  by a subsonic solution. The behaviour in the subsonic regime is equivalent to that discussed in case (2a). The ever-expanding solutions are not represented in figures 9 and 10. However, they can be obtained from the ever-collapsing ones (dashed curves) by letting  $z \rightarrow -z$  and  $V \rightarrow -V$ .

### 3.4. The asymptotically Minkowski solutions for $\alpha > \frac{1}{5}$

In this section we will discuss the ‘asymptotically Minkowski’ solutions, a class of self-similar solutions that were only discovered very recently and are of particular relevance to critical phenomena, see [10] for further details. These were missed in CC’s original asymptotic analysis, although they were able to extend their work after GNU had demonstrated the existence of such solutions. By combining the two approaches, we gain further physical insights into their significance. There are actually two families of asymptotically Minkowski solutions and both are only physical for  $\alpha > \frac{1}{5}$ :

A) The first family is described by two parameters and is associated with the equilibrium points M in state space. The solutions in this family have  $|V| \rightarrow 1$ ,  $S \rightarrow \infty$  and  $\mu \rightarrow 0$  at some *finite* value  $z = z_*$ . In this limit,

$$\dot{V}/V = -(5\alpha - 1)/(1 - \alpha). \quad (7)$$



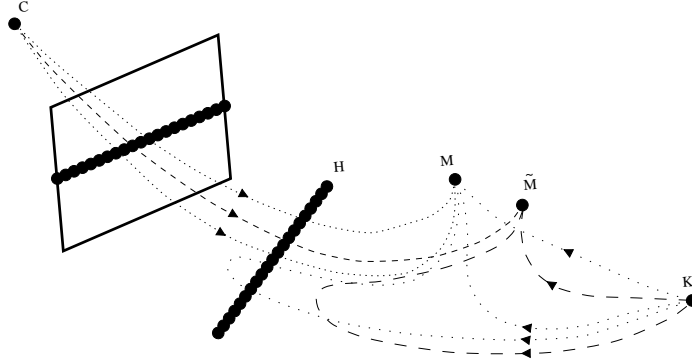


**Figure 11.** Asymptotically Minkowski solutions of class A (dotted) and class B (dashed) as orbits in state space. Densely dotted and short-dashed curves correspond to regular solutions, while sparsely dotted and long-dashed curves correspond to singular solutions.

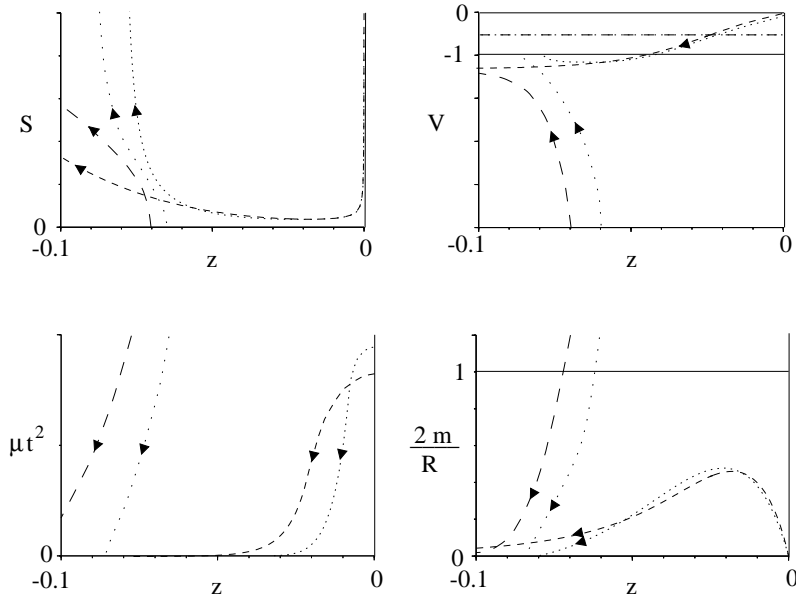


**Figure 12.** Physical quantities for asymptotically Minkowski solutions. The dash-dotted line in the  $V(z)$  diagram corresponds to the sonic line. Other designations are given in the caption of figure 11. The relation to the state space is as follows:  $S \rightarrow 0$ ,  $|V| \rightarrow \infty$ ,  $\mu t^2 \rightarrow \infty$ ,  $2m/R \rightarrow \infty$  corresponds to non-isotropic singularities (K points);  $S \rightarrow \infty$ ,  $V \rightarrow 0$ ,  $\mu t^2$  finite,  $2m/R \rightarrow 0$  as  $z \rightarrow 0$  correspond to infinitely dispersed solutions (C points);  $S \rightarrow \infty$ ,  $V$  finite,  $\mu t^2 \rightarrow 0$ ,  $2m/R \rightarrow 0$  with  $z \neq 0$  correspond to the asymptotically Minkowski solutions (M,  $\tilde{M}$  points).

This family is illustrated by the dotted curves in figures 11 and 12. Although the value of  $z$  is finite at the M point, it should be noted out that the Schwarzschild radial distance ( $R = rS$ ) is infinite. This is clearly seen in figure 12, where  $S$  goes to infinity for finite values of  $z$ .

B) The second family is described by one parameter and is associated with the equilibrium points  $\pm\tilde{M}$  in state space. The solutions in this family have  $|V| \rightarrow V_* > 1$ ,  $S \rightarrow \infty$  and  $\mu \rightarrow 0$  as  $z \rightarrow \infty$ . The expression for  $V_*$  is

$$V_* = \frac{\alpha(\alpha + 1) + \sqrt{\alpha(\alpha^3 - \alpha^2 + 3\alpha + 1)}}{1 - \alpha}. \quad (8)$$

In figures 11 and 12, the dashed curves correspond to this family of solutions.

Both families of solutions have  $2m/R \rightarrow 0$  as a solution approaches M or  $\tilde{M}$ . However, even though  $2m/R \rightarrow 0$  as one approaches M, the mass  $m$  need not vanish. It is important to realize that these solutions are not asymptotically flat in the usual sense. Rather, they are perfect-fluid spacetimes for which the Minkowski geometry is obtained asymptotically along certain coordinate lines. This is reminiscent of the open Friedmann solutions, which asymptotically approaches the Milne model along certain timelines (see, e.g., [16]).

As can be seen in figures 11 and 12, both families contain solutions that can be connected either to the origin  $z = 0$  (via a sonic point) or to a non-isotropic singularity (for which  $S \rightarrow 0$  at finite values  $z_K$ ). The former are of type TS, while the latter are of type S or STS, using the classification of section 3.1. For both families, the limit  $S \rightarrow \infty$  can be regarded as corresponding to an infinitely dispersed state, analogous to the late stage of an open Friedmann model, which is described by the Milne solution, see, e.g., [16].

Note that there is a 1-parameter family of non-isotropic singularity solutions for each value of  $z_K$  (i.e., one can take one of the two parameters that specify the solutions near K to be the value of the similarity variable at K). Most of these will be asymptotic to either a type A asymptotically Minkowski solution or a quasi-static solution. However, for sufficiently large values of  $|z_K|$ , there will also be one type B asymptotically Minkowski solution and one asymptotically Friedmann solution, all connected with K. The limiting value of  $z_K$  is the same in each case, reflecting the fact that the conditions at large values of  $|z|$  have little influence on what happens near the singularity. This limiting value corresponds to the splitting of the asymptotically Friedmann and asymptotically  $\tilde{M}$  submanifolds: the orbits belonging to each separatrix surface can be described by one parameter. For some ranges of this parameter they are asymptotic to a K equilibrium point, corresponding to a non-isotropic singularity; for other ranges they have a sonic point. This is illustrated for the asymptotically Minkowski solutions in figure 11, where dashed curves correspond to type B solutions. The analogous behaviour of the asymptotically Friedmann solutions can be seen in figure 7.

#### 4. Examples of equation-of-state dependent features

There are several features of the solutions that depend on the equation-of-state parameter  $\alpha$ . In particular, the behaviour at the sonic line is greatly affected by the equation of state. Below, we list some of these equation-of-state dependent features.

- $\alpha \approx 0.04$ : The boundary of the underdense subsonic band (see subsection 3.2) changes with increasing  $\alpha$  from being the general-relativistic Penston-Larson solution to the degenerate node in the nodal region containing the flat Friedmann solution (i.e.,  $z = z_3$ ).
- $\alpha \approx 0.11$ : The upper boundary (as defined by OP) of the first overdense subsonic band changes with increasing  $\alpha$  from being a secondary eigenvector direction in the nodal region containing the static solution to the degenerate node of that nodal region (i.e.,  $z = z_2$ ).
- $\alpha = \frac{1}{5}$ : The equilibrium points  $\tilde{M}^+$  leave each timelike SSS state space and enter the spatially SSS state space as the equilibrium points  $\pm\tilde{M}$ .
- $\alpha \approx 0.28$ : The critical solution, which corresponds to the lower boundary of the first overdense subsonic band, changes character with increasing  $\alpha$  from a solution with a (generally irregular) second sonic point to a solution whose corresponding orbit ends at an M point in the spatially SSS state space. For the threshold value of  $\alpha$ , the critical solution ends at an  $\tilde{M}$  point.
- $\alpha = \frac{1}{3}$ : The degenerate nodes of the nodal regions of the sonic line coincide with, respectively, the flat Friedmann solution and the static solution (i.e.,  $z_F = z_3$  and  $z_S = z_2$ ).

The eigenvector direction at the sonic line of the flat Friedmann solution changes with increasing  $\alpha$  from being a dominant direction to a secondary direction. For the static solution, the situation is reversed: the eigenvector direction going from being secondary to dominant.

The boundary of the underdense subsonic band changes with increasing  $\alpha$  from being the degenerate node in the nodal region containing the flat Friedmann solution to the flat Friedmann solution itself (i.e.,  $z = z_F$ ).

- $\alpha \approx 0.41$ : The eigenvector direction associated with the critical solution at the sonic line changes with increasing  $\alpha$  from being an attractive eigenvector direction in the saddle region of the sonic line to a secondary eigenvector direction in the nodal region containing the static solution (i.e.,  $z_1 < z < z_2$ ).
- $\alpha \approx 0.45$ : The overdense subsonic bands overlap, so that the band structure degenerates to only two bands: the underdense band and one overdense band.
- $\alpha \approx 0.61$ : The zero in the radial 3-velocity  $V_R$  of the critical solution changes with increasing  $\alpha$  from being subsonic to being supersonic (i.e., for this value of  $\alpha$ ,  $V_R = 0$  when  $|V| = \sqrt{\alpha}$ ).
- $\alpha \approx 0.89$ : The eigenvector direction associated with the critical solution at the sonic line coincides with the degenerate node in the nodal region associated with the static solution (i.e.,  $z = z_2$ ), and changes with increasing  $\alpha$  from being a secondary eigenvector direction to a dominant eigenvector direction.

## 5. Concluding remarks

It is clear from the present work that we are close to a complete understanding of the self-similar spherically symmetric solutions. This paper has emphasized the advantages of a combined comoving and homothetic approach. This is particularly clear in the investigations of the asymptotically quasi-static solutions and asymptotically Minkowski solutions.

An important application is to study the critical solution of spherically symmetric perfect-fluid collapse. This has been done in a separate paper [10], where it is shown that the critical solution is the unique self-similar solution which is analytic at the sonic point, has a regular centre, and contains one collapsing region surrounded by a dispersing exterior. As indicated in section 4, this solution is a member of the asymptotically quasi-static class for  $0 < \alpha \lesssim 0.28$ , a member of the asymptotically Minkowski class of type B for  $\alpha \approx 0.28$ , and a member of the asymptotically Minkowski class of type A for  $0.28 \lesssim \alpha < 1$ .

Possible future investigations involve studying these models in more general contexts. One might ask if various features discussed here are structurally stable, i.e., how do other geometries and matter sources affect the behaviour? For example, one might further examine the role of the self-similar solutions in the complete space of spherically symmetric solutions. It also remains to consider the stiff fluid ( $\alpha = 1$ ) case, which is of relevance in the study of massless scalar fields. There are numerous bifurcations associated with the limit  $\alpha \rightarrow 1$  and this explains the numerical problems one encounters in this limit. However, we do not see any *a priori* analytic difficulties in studying these models using the methods presented in this paper.

## Acknowledgements

We would like to thank Dave Neilsen for helpful comments. AAC was supported by the Natural Sciences and Engineering Research Council of Canada. CU was supported by the Swedish Natural Research Council.

## Appendix A. Equations

This appendix collects the basic equations in each approach, together with expressions for the physically interesting quantities that we have used.

### Appendix A.1. Comoving equations

The field equations (with  $G = c = 1$ ) reduce to a set of ordinary differential equations in  $x$  and  $S$ :

$$\ddot{S} + \dot{S} + \left( \frac{2}{1+\alpha} \frac{\dot{S}}{S} - \frac{1}{\alpha} \frac{\dot{x}}{x} \right) [S + (1+\alpha)\dot{S}] = 0, \quad (\text{A.1})$$

$$\begin{aligned} & \left( \frac{2\alpha\gamma^2}{1+\alpha} \right) S^4 + \frac{2}{\beta^2} \frac{\dot{S}}{S} x^{2(1-\alpha)/\alpha} z^{2(1-\alpha)/(1+\alpha)} - \\ & \gamma^2 S^4 \frac{\dot{x}}{x} \left( \frac{V^2}{\alpha} - 1 \right) = (1+\alpha)x^{(1-\alpha)/\alpha}, \end{aligned} \quad (\text{A.2})$$

$$M = S^2 x^{-(1+\alpha)/\alpha} \left[ 1 + (1+\alpha) \frac{\dot{S}}{S} \right], \quad (\text{A.3})$$

$$M = \frac{1}{2} + \frac{1}{2\beta^2} x^{-2} z^{2(1-\alpha)/(1+\alpha)} \dot{S}^2 - \frac{1}{2} \gamma^2 x^{-(2/\alpha)} S^6 \left( 1 + \frac{\dot{S}}{S} \right)^2, \quad (\text{A.4})$$

where an overdot denotes  $z d/dz$ . At any point in the  $(x, S, \dot{S})$  space, for a fixed value of  $\alpha$ , equations (A.3) and (A.4) provide a constraint that gives the value of  $z$ ; equation (A.2) then gives the value of  $\dot{x}$  unless  $|V| = \sqrt{\alpha}$  and equation (A.1) gives the value of  $\dot{S}$ . Thus the equations generate a vector field  $(\dot{x}, \dot{S}, \dot{S})$  and this specifies an integral curve at each point of the 3-dimensional space, each curve representing one particular similarity solution.

Where  $|V| = \sqrt{\alpha}$ , equations (A.3, A.4) together with the expression for  $V(z)$  [see equation (A.19)] allow one to express  $\dot{S}$  in terms of  $x$  and  $S$ , corresponding to a surface in  $(x, S, \dot{S})$  space. Integral curves intersect  $|V| = \sqrt{\alpha}$  in a physically reasonable manner only if

$$\begin{aligned} & \left( \frac{2\alpha\gamma^2}{1+\alpha} \right) S^4 + \frac{2}{\beta^2} \frac{\dot{S}}{S} x^{(2-2\alpha)/\alpha} z^{(2-2\alpha)/(1+\alpha)} \\ & = (1+\alpha) x^{(1-\alpha)/\alpha}, \end{aligned} \quad (\text{A.5})$$

since otherwise the value of  $\dot{x}$  and hence the pressure, density and velocity gradient diverge there. Since equation (A.5) corresponds to another 2-dimensional surface in  $(x, S, \dot{S})$  space, this will intersect the surface  $|V| = \sqrt{\alpha}$  on a line Q, the sonic line.

#### Appendix A.2. Homothetic equations

Here, we briefly summarize the quantities and equations used in the diagonal homothetic approach. In the spatially self-similar case, the dependent variables  $(\bar{Q}_0, \bar{Q}_+, \bar{C}_1, v)$  are defined in terms of the line element

$$ds^2 = e^{2X} \frac{3}{Y^2} \left[ d\tau^2 - \frac{dX^2}{C_1^2} - \frac{d\Omega^2}{(1-\bar{Q}_0^2)} \right], \quad (\text{A.6})$$

together with  $\bar{Q}_+ = -D'_1/D_1 = Y'/Y + \bar{C}'_1/\bar{C}_1$  and  $v = 1/V$ , where  $' = d/d\tau$ .  $Y$  is given by the decoupled equation

$$Y' = - \left\{ \bar{Q}_+ + \bar{Q}_0 \left[ 2\bar{Q}_+^2 + \frac{1+\alpha}{1+\alpha v^2} \Omega_n \right] \right\} Y. \quad (\text{A.7})$$

The Friedmann equation defines  $\Omega_n$ :

$$\Omega_n = 1 - \bar{Q}_+^2 - \bar{C}_1^2. \quad (\text{A.8})$$

The constraint takes the form

$$G = (1+\alpha)v\Omega_n - 2[1+\alpha v^2]\bar{Q}_+\bar{C}_1 = 0. \quad (\text{A.9})$$

The reduced set of evolution equations is

$$\begin{aligned}
\bar{Q}_0' &= -(1 - \bar{Q}_0^2) \left[ \bar{Q}_+^2 - \bar{C}_1^2 + \frac{\alpha(1 - v^2)}{1 + \alpha v^2} \Omega_n \right], \\
\bar{Q}_+' &= -\bar{Q}_0 \bar{Q}_+ \left[ 2(1 - \bar{Q}_+^2) - \frac{(1 + \alpha)\Omega_n}{1 + \alpha v^2} \right] \\
&\quad - \frac{1(1 - \alpha) + (3\alpha + 1)v^2}{2(1 + \alpha v^2)} \Omega_n, \\
\bar{C}_1' &= 2\bar{C}_1 \left[ \bar{Q}_+ + \bar{Q}_0 \bar{Q}_+^2 + \frac{1}{2} \frac{1 + \alpha}{1 + \alpha v^2} \bar{Q}_0 \Omega_n \right], \\
v' &= \frac{1 - v^2}{(1 + \alpha)[1 - \alpha v^2]} \left\{ (1 + \alpha) [2\alpha \bar{Q}_0 + (1 + \alpha)\bar{Q}_+] v \right. \\
&\quad \left. + [\alpha(3\alpha + 1)v^2 - (1 - \alpha)] \bar{C}_1 \right\}. \tag{A.10}
\end{aligned}$$

In the timelike self-similar case, the dependent variables  $(\bar{\Sigma}_+, \bar{A}, \bar{K}, V)$  are defined in terms of the line element

$$ds^2 = e^{2T} \frac{3}{\bar{\theta}^2} \left[ \frac{dT^2}{\bar{A}^2} - d\xi^2 - \frac{d\Omega^2}{\bar{K}} \right], \tag{A.11}$$

together with  $\bar{\Sigma}_+ = -D_1'/D_1 = \bar{\theta}'/\bar{\theta} + \bar{A}'/\bar{A}$ , where  $' = d/d\xi$ .  $\bar{\theta}$  is given by the decoupled equation

$$\bar{\theta}' = - \left[ 1 + \bar{\Sigma}_+(1 + \bar{\Sigma}_+) - \bar{A}^2 - \frac{\alpha(1 - V^2)}{1 + \alpha V^2} \Omega_t \right] \bar{\theta}. \tag{A.12}$$

The Friedmann equation defines  $\Omega_t$ :

$$\Omega_t = \frac{1 + \alpha V^2}{V^2 + \alpha} (1 - \bar{\Sigma}_+^2 - \bar{A}^2 - \bar{K}). \tag{A.13}$$

The constraint takes the form

$$G = (1 + \alpha)V\Omega_t - 2[1 + \alpha V^2] \bar{\Sigma}_+ \bar{A} = 0. \tag{A.14}$$

The reduced set of evolution equations is

$$\begin{aligned}
\bar{\Sigma}_+' &= -\bar{\Sigma}_+ \left[ 1 - \bar{\Sigma}_+^2 + \bar{A}^2 + \frac{\alpha(1 - V^2)}{1 + \alpha V^2} \Omega_t \right] \\
&\quad - \frac{1(3\alpha + 1) + (1 - \alpha)V^2}{2(1 + \alpha V^2)} \Omega_t, \\
\bar{A}' &= \left[ 1 + 2\bar{\Sigma}_+ + \bar{\Sigma}_+^2 - \bar{A}^2 - \frac{\alpha(1 - V^2)}{1 + \alpha V^2} \Omega_t \right] \bar{A}, \\
\bar{K}' &= 2 \left[ \bar{\Sigma}_+^2 - \bar{A}^2 - \frac{\alpha(1 - V^2)}{1 + \alpha V^2} \Omega_t \right] \bar{K}, \\
V' &= \frac{1 - V^2}{(1 + \alpha)[V^2 - \alpha]} \left\{ (1 + \alpha) [2\alpha + (1 + \alpha)\bar{\Sigma}_+] V \right. \\
&\quad \left. + [\alpha(3\alpha + 1) - (1 - \alpha)V^2] \bar{A} \right\}. \tag{A.15}
\end{aligned}$$

Note that  $V$  was denoted by  $u$  in GNU2.

## Appendix A.3. Physical quantities

Here, we give the expressions for the different physically interesting quantities we have used. First we note that in the homothetic approach, the similarity variable  $z = r/t$  is

$$\begin{aligned} z &\propto \text{sgn}(v)e^{-\sqrt{3} \int d\tau Y^{-1}} \\ &\propto \text{sgn}(V)e^{\sqrt{3} \int d\xi \bar{\theta}^{-1}}, \end{aligned} \quad (\text{A.16})$$

where equation (3) and the transformations between the comoving and homothetic approaches (see GNU1,2) have been used.

The scale factor  $S \equiv R/r$  is one of CC's dependent variables. In the homothetic approach, it is determined by

$$\begin{aligned} S^2(z) &\propto |z|^{-(1-\alpha)/(1+\alpha)} \frac{\bar{C}_1}{|\bar{Q}_+|} \\ &\propto |z|^{-(1-\alpha)/(1+\alpha)} \frac{\bar{A}}{|\bar{\Sigma}_+|}. \end{aligned} \quad (\text{A.17})$$

GNU use the velocity function (or its inverse) as one of their dependent variables. It can be covariantly expressed in terms of the fluid 4-velocity  $u^\alpha$  and the normal to the homothetic symmetry surfaces  $n^\alpha$  as follows [1]

$$V = \frac{u^\alpha n_\alpha}{\sqrt{(u^\alpha n_\alpha)^2 - n^\alpha n_\alpha}}. \quad (\text{A.18})$$

In the comoving variables used here,  $V$  takes the form

$$V = (\beta\gamma)^{-1} x^{(1-\alpha)/\alpha} S^{-2} z^{(1-\alpha)/(1+\alpha)}. \quad (\text{A.19})$$

The expressions for the density profile are

$$\begin{aligned} \mu t^2 &= \frac{1}{4\pi} z^{-2} x^{-(1+\alpha)/\alpha} \\ &= S^{-2} z^{-2} \frac{1-v^2}{1+\alpha v^2} \frac{\Omega_n}{1-\bar{Q}_0^2} \\ &= S^{-2} z^{-2} \frac{1-V^2}{1+\alpha V^2} \frac{\Omega_t}{\bar{K}}. \end{aligned} \quad (\text{A.20})$$

The mass function is defined as  $M \equiv m/R$  where

$$m(r, t) = \frac{1}{2} R \left[ 1 + e^{-2\nu} \left( \frac{\partial R}{\partial t} \right)^2 - e^{-2\lambda} \left( \frac{\partial R}{\partial r} \right)^2 \right], \quad (\text{A.21})$$

or equivalently

$$m(r, t) = 4\pi \int_0^r \mu R^2 \frac{\partial R}{\partial r'} dr'. \quad (\text{A.22})$$

In the comoving approach, it is given by either of equations (A.3,A.4), while in the homothetic approach it takes the forms

$$\begin{aligned} M &= \frac{1 + 2\bar{Q}_0\bar{Q}_+ + \bar{Q}_+^2 - \bar{C}_1^2}{2(1 - \bar{Q}_0^2)} \\ &= \frac{\bar{K} - (1 + \bar{\Sigma}_+)^2 + \bar{A}^2}{2\bar{K}}. \end{aligned} \quad (\text{A.23})$$

Finally, the asymptotic energy per unit mass  $E$  is the limit  $|z| \rightarrow \infty$  of the dimensionless quantity  $\mathcal{E}$ , which represents the total energy per unit mass of a comoving shell:

$$\begin{aligned} \mathcal{E} &= \frac{1}{2} \left\{ \gamma^2 x^{-2/\alpha} S^6 \left( 1 + \frac{\dot{S}}{S} \right) - 1 \right\} \\ &= \frac{1}{2} \left\{ \frac{[v(\bar{Q}_0 + \bar{Q}_+) + \bar{C}_1]^2}{(1 - \bar{Q}_0^2)(1 - v^2)} - 1 \right\} \\ &= \frac{1}{2} \left\{ \frac{(1 + \bar{\Sigma}_+ + \bar{A}V)^2}{\bar{K}(1 - V^2)} - 1 \right\}. \end{aligned} \tag{A.24}$$

## References

- [1] Cahill M E and Taub A H 1971 *Commun. Math. Phys.* **21** 1
- [2] Bogoyavlensky O I 1985 *Methods in the qualitative theory of dynamical systems in astrophysics and gas dynamics* (Berlin: Springer)
- [3] Anile A M, Moschetti G and Bogoyavlenski O I 1987 *J. Math. Phys.* **28** 2942
- [4] Goliath M, Nilsson U S, and Uggla C 1998 *Class. Quant. Grav.* **15** 167
- [5] Goliath M, Nilsson U S, and Uggla C 1998 *Class. Quant. Grav.* **15** 2841
- [6] Carr B J 2000 *Phys. Rev. D* **62** 044022
- [7] Carr B J and Coley A A 2000 *Phys. Rev. D* **62** 044023
- [8] Carr B J and Coley A A 2000 *An asymptotic analysis of spherically symmetric perfect fluid self-similar solutions*, to appear in *Class. Quantum Grav.*
- [9] Ori A and Piran T 1990 *Phys. Rev. D* **42** 1068
- [10] Carr B J, Coley A A, Goliath M, Nilsson U S and Uggla C 2000 *Phys. Rev. D* **61** 081502
- [11] Bicknell G V and Henriksen R N 1978 *Astrophys. J.* **225** 237
- [12] Foglizzo T and Henriksen R N 1993 *Phys. Rev. D* **48** 4645
- [13] Carr B J and Yahil A 1990 *Astrophys. J.* **360** 330
- [14] Eardley D M 1974 *Commun. Math. Phys.* **37** 287
- [15] Defrise-Carter L 1975 *Commun. Math. Phys.* **40** 273
- [16] Wainwright J and Ellis G F R 1997 *Dynamical systems in cosmology* (Cambridge: Cambridge University Press)
- [17] Hewitt C G and Wainwright J 1992 *Phys. Rev. D* **46** 4242
- [18] Nilsson U and Uggla C 1996 *Class. Quant. Grav.* **13** 1601
- [19] Carr B J and Hawking S W 1974 *Mon. Not. Roy. Astr. Soc.* **168** 399
- [20] Bicknell G V and Henriksen R N 1978 *Astrophys. J.* **219** 1043
- [21] Lin D N C, Carr B J and Fall S D M 1978 *Mon. Not. Roy. Astr. Soc.* **177** 51